SOAR - Satellite for Orbital Aerodynamics Research

SOAR – Satellite for Orbital Aerodynamics Research

N.H. Crisp[a,*], P.C.E. Roberts[a], S. Edmondson[a], S.J. Haigh[a], C. Huyton[a], S. Livadiotti[a], V.T.A. Oiko[a], K.L. Smith[a], S.D. Worrall[a], J. Becedas[b], D. González[b], G. González[b], R. Domínguez[b], K. Bay[c], L. Ghizoni[c], V. Jungnell[c], J. Morsbøl[c], T. Binder[d], A. Boxberger[d], S. Fasoulas[d], G.H. Herdrich[d], F. Romano[d], C. Traub[d], D. Garcia-Almiñana[e], S. Rodriguez-Donaire[e], M. Sureda[e], D. Kataria[f], R. Outlaw[g], B. Belkouchi[h], A. Conte[h], J.S. Perez[h], R. Villain[h], A. Heißerer[i], A. Schwalber[i]

[a] *The University of Manchester, Oxford Rd, Manchester, M13 9PL, United Kingdom*
[b] *Elecnor Deimos Satellite Systems, Calle Francia 9, 13500 Puertollano, Spain*
[c] *GomSpace AS, Langagervej 6, 9220 Aalborg East, Denmark*
[d] *University of Stuttgart, Pfaffenwaldring 29, 70569 Stuttgart, Germany*
[e] *UPC-BarcelonaTECH, Carrer de Colom 11, 08222 Terrassa, Barcelona, Spain*
[f] *Mullard Space Science Laboratory (UCL), Holmbury St. Mary, Dorking, RH5 6NT, United Kingdom*
[g] *Christopher Newport University, Newport News, Virginia 23606, USA*
[h] *Euroconsult, 86 Boulevard de Sébastopol, 75003 Paris, France*
[i] *concentris research management gmbh, Ludwigstraße 4, D-82256 Fürstenfeldbruck, Germany*

Abstract

SOAR (Satellite for Orbital Aerodynamics Research) is a CubeSat mission designed to investigate the interaction between different materials and the atmospheric flow regime in Very Low Earth Orbits (VLEO) and to demonstrate aerodynamic attitude and orbit control manoeuvres. Improving knowledge of the gas-surface interactions is important for the design of future satellites operating in lower altitude orbits and will enable the identification of materials which can minimise drag or improve aerodynamic control, a key aim of the Horizon 2020 DISCOVERER project. In order to achieve these objectives, SOAR features two payloads: i) a set of steerable fins which provide the ability to expose different materials or surface finishes to the oncoming flow with varying angle of incidence whilst also providing variable geometry to investigate aerostability and aerodynamic control; and ii) an Ion and Neutral Mass Spectrometer with Time-of-Flight capability which enables accurate measurement of the in-situ flow composition, density, and thermospheric wind velocity. Using precise orbit and attitude determination information and the measured atmospheric flow characteristics the drag and side-force experienced by the satellite in orbit can studied and estimates of the aerodynamic coefficients calculated. This paper first presents the scientific design and operational concept of the SOAR mission, focusing on the stability and control strategy which enables the spacecraft to maintain the flow-pointing attitude required by the payloads. The methodology for recovery of the (relative) aerodynamic coefficients from the measured orbit and in-situ atmospheric data is then presented. Finally, the uncertainty of the resolved aerodynamic coefficients is estimated statistically using simulations.

Keywords: Orbital Aerodynamics; Drag Coefficient; Gas-Surface Interactions; Thermospheric Wind; CubeSat.

1. Introduction

SOAR (Satellite for Orbital Aerodynamics Research) is a scientific CubeSat mission designed to investigate the interactions between the atmospheric flow regime in Very Low Earth Orbits (VLEO) and different materials and surface-coatings. Secondary objectives of the SOAR mission are to provide new in-situ measurements of the atmospheric density and composition and variation of the thermospheric wind velocity over the range of altitudes below approximately 400 km. SOAR will also demonstrate novel attitude and orbit control manoeuvres using the aerodynamic forces and torques which can be generated at these altitudes.

The SOAR mission is a key component of to Horizon 2020 funded DISCOVERER project [1], which aims to radically redesign Earth Observation satellites for sustained operation at significantly lower altitudes. Improving the knowledge and understanding of the Gas-Surface Interactions (GSIs) at these low orbital altitudes is an important step in the identification of novel and interesting materials which can reduce atmospheric drag or improve aerodynamic control capability.

The experiments performed by SOAR will be used to provide valuable validation data for further ground-based experiments on materials and GSIs which will be performed in the ROAR (Rarefied Orbital Aerodynamics Research) Facility [1] at The University of Manchester. The

*Corresponding author.
Email address: nicholas.crisp@manchester.ac.uk (N.H. Crisp)

Nomenclature

α	Energy accommodation coefficient	C_F	Force Coefficient
$\ddot{\theta}$	Rotational acceleration	C_T	Torque Coefficient
$\ddot{x}$	Linear acceleration	I	Moment of inertia
ρ	Atmospheric density	l_{ref}	Reference length
$\vec{v_{rel}}$	Relative atmospheric flow vector	m	Mass
A_{ref}	Reference area	R_a	Earth equatorial radius

ROAR Facility is a unique set-up which is aimed at the identification of novel materials for satellite applications with a focus on improved aerodynamic properties and atomic oxygen resistance. The facility is principally comprised of a UHV environment, an atomic oxygen source capable of providing representative orbital velocities and surface interactions, and a sensor suite including Ion and Neutral Mass Spectrometers (INMS) which enable measurement and characterisation of the incident and reemitted gas-flow on sample materials.

1.1. The VLEO Environment

Very Low Earth Orbits can be defined as those below which the atmosphere begins to have a meaningful effect on the orbital and attitude dynamics of a spacecraft. In comparison to Low Earth Orbits (LEO), typically defined as any orbit below 2000 km, VLEO is generally defined as below 500 km to 450 km. However, this definition may be somewhat deceptive as in reality the range of VLEO varies with density and the expansion and contraction of the atmosphere and is therefore highly dependent on the solar cycle. The lower-end of the VLEO range is bounded by orbits which can be sustained for a very short period of time as a result of the significant atmospheric drag which will be acting at these altitudes, typically between 100 km to 150 km.

In VLEO the atmosphere is significantly less dense than the ground or conventional flight altitudes and is considered to be rarefied such that the mechanics of continuum flow regimes can no longer be applied. The non-dimensional Knudsen number can be used to classify different flow-regimes and is defined as the ratio between the mean free path (the average distance between successive collisions) of the constituent molecules in a flow and a characteristic physical length (eg. the length of a body in that flow). When the Knudsen number is high (ie. $Kn > 10$) the gas-surface interactions along the length of a body are of much greater significance than any gas-gas interactions, including those with reflected particles [2]. This regime is termed Free Molecular Flow (FMF), and generally applies across the VLEO range for spacecraft of typical size [3].

In the FMF regime of VLEO the interactions between molecules (incident and reflected) are considered to have a negligible effect on the flow. The forces which act on a body can therefore be determined by considering only the interactions between the molecules and the body, and in particular the momentum and energy transfer which occurs at the surface. It is known that these interactions are dependent on surface roughness and cleanliness (particularly related to altitude-dependent atomic oxygen adsorption and accommodation), surface composition and lattice structure, surface temperature, gas composition, and the incident particle temperature, velocity, and incidence angle [4, 5, 6]. However, whilst numerous models for these GSIs and the associated force coefficients have been developed [2, 7, 8, 9, 10], most of these factors have thus far been neglected. A key element of this current deficit in GSI modelling is the lack of experimentation which can offer insight into the effect that each of these factors has on the momentum and energy transfer in a GSI and therefore the forces which act on a body in the VLEO flow regime.

1.2. On-Orbit Investigation of Gas-Surface Interactions in VLEO

Previous investigation of gas-surface interactions in the FMF regime has included both experimentation performed in laboratories and on-orbit, review of which is principally provided by Moe et al. [4], Moe and Moe [11] and Pilinski [12]. Some studies have used indirect measurement techniques, for example investigating adsorption on pressure gauge and mass spectroscopy instruments [13], or passive detection of scattered remission angle [14, 15]. However, systematic and sustained experimental campaigns have not yet been carried out and measurement of external spacecraft surface accommodation has not yet been approached. Whilst direct measurement of the experienced drag forces using accelerometers has been performed during the transitional re-entry phase of the Space Shuttle [16, 17], further experiments in the wider LEO range have not yet been pursued.

Other studies have used observational methods to infer fitted accommodation and drag coefficients of different spacecraft or materials from the attitude motion or orbital trajectory. These experiments have notably included Paddlewheel [18] and spherical [5, 19] satellites, but have also included more complex geometries [20, 21, 22]. However,

the results obtained using these methods have thus far relied on modelled atmospheric densities and are therefore subject to their inherent biases and uncertainties.

By analysis of the ODERACS radar calibration satellites, [19] suggest that the variation in fitted drag coefficient for similar spherical geometries with varying surface composition or treatment is less than 5 % in VLEO at solar minimum and that this variation reduces with altitude as a result of increased atomic oxygen adsorption.

1.3. Scientific Objectives

The principal scientific objective of SOAR is to investigate the variation of the aerodynamic coefficients of different materials and surface finish at different incidence angle to the oncoming flow and at different orbital altitudes. In-situ measurement techniques will be used to provide knowledge of the incident flow environment in addition to the attitude and orbital parameters from which the forces and torques experienced by the body can be recovered. By providing in-situ density measurements of the oncoming flow which can be used directly in the recovery of the fitted aerodynamic coefficients and associated accommodation coefficients, this experimental methodology presents a significant advantage over previous observation-based studies.

The additional mission objectives for SOAR are as follows, but beyond the scope of this paper.

- Perform measurements of the thermospheric wind speed and vector.
- Perform measurement of atmospheric density and composition.
- Demonstrate the ability to control the spacecraft attitude using aerodynamic torques.
- Demonstrate the ability to control the spacecraft orbit using aerodynamic forces.

2. Satellite Design

SOAR takes the form of a 3U CubeSat developed from the ΔDsat design of Virgili Llop and Roberts [23], previously proposed for the QB50 programme for lower thermospheric exploration and research. The basic geometry and configuration of SOAR is shown in Fig. 1.

In order to provide in-situ information about the flow conditions, including thermospheric winds, the spacecraft features a forward-facing Ion and Neutral Mass Spectrometer (INMS). This sensor, improved since the development of the QB50 satellites, includes new Time-of-Flight (ToF) capability, enabling assessment of the incoming flow velocity in addition to the total atmospheric density and flow composition.

To maintain accuracy of the INMS instrument, the spacecraft must be pointed in the direction of the oncoming flow to within a given acceptance angle. Simply, this requires that the spacecraft nominally flies in an attitude which is aligned with the direction of the flow. SOAR therefore features a similar design of four aerodynamic panels as ΔDsat, providing natural aerostability to the spacecraft. These panels can also be rotated to achieve the scientific objectives of the mission and are therefore termed steerable-fins herein.

Figure 1: Geometry and configuration of the SOAR satellite with steerable fins and INMS payloads.

The surfaces of these steerable-fins will coated with different materials and surface finishes and will be exposed to the flow at varying angles of incidence to perform the proposed investigation of the drag and lift coefficients. As described by Virgili Llop and Roberts [23], the steerable-fins can be operated in pairs in two different ways; co-rotation and counter-rotation. Under stable flow-pointing conditions, co-rotation of a single pair of the steerable-fins creates a net lift or side force and therefore a torque (in yaw for the vertical fins or pitch for the lateral fins). The spacecraft will therefore rotate to fly at an angle to the flow. Contrastingly, counter-rotation of a pair of opposing fins generates no net side-force, but creates a torque-couple in roll, causing the spacecraft to spin about the flow-pointing direction.

Attitude control of the spacecraft is principally enabled by a three-axis reaction wheel assembly (tetrahedral configuration of four wheels). A three-axis magnetorquer is also specified to perform initial detumbling operations following launch and to enable desaturation and momentum management of the reaction wheels. SOAR also carries a nanosatellite-class star-tracker and Earth and sun sensors

to provide precise attitude knowledge. An on-board GPS receiver provides the precise position and velocity of the spacecraft and removes dependency of the experiment on observational tracking information.

3. Experimental Design

A body exposed to an oncoming flow will produce force of an aerodynamic nature, the magnitude and direction of which will be dependant on the orientation with respect to the flow vector. This force is often decomposed into three mutually perpendicular forces; drag, normal, and side force. An alternative term, lift force, is often used to refer to either the normal or side force depending on the convention used the chosen coordinate system. Using Eq. (1) each of these forces can be associated with a dimensionless force coefficient C_F which relates the magnitude of the force or accelerations produced with the dynamic pressure of the surrounding flow and the spacecraft geometry.

$$F = \frac{1}{2}\rho v_{rel}^2 \frac{\vec{v_{rel}}}{|\vec{v_{rel}}|} A_{ref} C_F = m\ddot{x} \tag{1}$$

where ρ is the local atmospheric density, v_{rel} the spacecraft velocity relative to the oncoming flow, and A_{ref} the reference area.

Equivalently, an associated aerodynamic torque or rotational acceleration experienced can be described by Eq. (2) in which C_T is the aerodynamic torque coefficients (in either roll, pitch, or yaw) and l_{ref} is an additional reference length.

$$T = \frac{1}{2}\rho v_{rel}^2 \frac{\vec{v_{rel}}}{|\vec{v_{rel}}|} A_{ref} l_{ref} C_T = I\ddot{\theta} \tag{2}$$

The primary scientific objective of SOAR is to provide in-situ measurements of the GSI characteristics of different materials and surface-coatings in the VLEO environment. These GSI characteristics will be investigated by considering the the variation in drag and lift forces produced by the steerable-fins which can be observed when different materials are individually exposed to the oncoming flow at varying incidence angle and at different altitudes as the orbit of SOAR decays.

Reconciliation of these force and torque coefficients with the true GSI mechanics still requires a model for the exchange of energy and momentum of the gas species with the surface and the associated reemission pattern. However, experimental determination of these aerodynamic coefficients provides valuable in-situ validation data for the experiments which will be performed in the ROAR Facility.

3.1. Drag Coefficient

Investigation of the drag coefficient of different materials exposed to the flow by the steerable fins was proposed by Virgili Llop and Roberts [23] for the ΔDsat mission. In this method, opposing steerable-fins are counter-rotated, nominally producing no net lift/side-force, but a net torque in roll, thus allowing the drag coefficient to be determined from the resulting spacecraft trajectory.

For SOAR both co-rotated and counter-rotated configurations of the steerable fins can be considered to perform experiments on the variation in drag coefficient with incidence angle and altitude. Using the reaction wheels, torques generated by aerodynamics or other disturbances can be compensated and thus the nominal direction of the satellite controlled for a period of time during an experiment or test-run.

During these test-runs the orbital parameters or trajectory of the spacecraft will vary depending on the oncoming flow conditions and spacecraft geometry with respect to the flow. For example, as the incidence angle of the of the steerable fins is increased towards the normal, the panel area exposed to the flow will also be increased. The drag experienced by the spacecraft for a given flow condition will also therefore increase and will be reflected in the rate of orbital decay. The drag coefficient for a given orbital altitude and configuration of the steerable fins can subsequently be recovered by considering the relationship between the produced drag force and the acceleration of the spacecraft, expressed by Eq. (1). However, it should be noted that the drag coefficient determined by this method is representative of the whole spacecraft in the given configuration and not specific to only the surfaces or materials of the steerable fins exposed to the flow.

In practice, this analysis can be performed by using an orbit determination process which is informed by the atmospheric density and spacecraft position and velocity which are measured over the period of the test-run. A parameter-fitting process is used to to find the best-fit drag coefficient which provides convergence between the measured trajectory and a mathematical model for the motion of the spacecraft.

The accuracy to which the drag coefficient can be determined by such a method is primarily dependent on the quality of the experimental data which can be obtained during each test-run (characterised by uncertainty or noise) and the fidelity of the mathematical model to which this will be compared to. Therefore, to measure the drag coefficient of two different configurations, it is necessary that the measured trajectories of the two test-runs can be distinguished from each other. Effectively, this imposes a minimum requirement on the noise or uncertainty in the measured data and the duration of each test-run.

The fidelity of the mathematical model used by the orbit determination process can also have an effect on the quality of the recovered drag coefficient. In order to provide convergence towards the measured trajectory using the free parameter fitting it is necessary that the model incorporates the relevant perturbations and their spatial and temporal variations over the duration of the test-run. However, the selection of necessary perturbations and modelling fidelity are related to the noise in the mea-

sured position and velocity. Perturbations which would cause variation in the trajectory of the spacecraft of less than the noise in the measured values can be safely neglected, simplifying the form of the mathematical model. The selection of these perturbations is explored further in Section 6.

3.2. Lift Force Coefficient

As various definitions and conventions for the forces acting on a vehicle exist, the term lift force will be used herein to describe any force which acts perpendicular to that of the drag force in the body-axes of a notional spacecraft. This also provides commonality in terminology for both the vertical and lateral fins for SOAR which are symmetrical in roll (about the z-axis) with respect to the satellite.

Similarly to the drag coefficient, the lift force coefficient of the different materials and surfaces exposed to the flow by the steerable fins will be investigated by analysis of the resulting spacecraft motion and a parameter fitting method to recover the aerodynamic coefficient.

For a counter-rotated configuration of opposing steerable-fins can be used to analyse the lift force coefficient. The equal but opposing lift forces produced by the opposing fins act as a couple to generate a net rolling torque on the spacecraft. The lift force coefficient can therefore be recovered by considering the evolution of the spacecraft attitude, principally in roll.

Alternatively, for a co-rotated configuration of opposing steerable fins, both a net lift force and pitch/yaw torque will be produced. Two methods for recovery of the lift force coefficient can therefore be considered. The first uses the produced lift force and can be performed by coordinated analysis of the orbital trajectory of the spacecraft requiring simultaneous parameter fitting of the drag coefficient and the lift force coefficient. However, as the lift force of known materials is typically a fraction of the drag-force, the ability to effectively infer the lift force coefficient from the measured orbital data may be limited. The second method exploits the pitch/yaw torque produced by the co-rotated configuration of the steerable fins and utilises both the resulting attitude motion of the spacecraft and angular momentum of the reaction wheels to determine the lift force coefficient.

Use of the attitude dynamics of the spacecraft to determine the lift force coefficient requires an expression relating the torque T produced by the steerable fins to the angular acceleration $\ddot{\theta}$ about a given axis of the spacecraft, given by Eq. (3).

$$T = F_L l_F = \frac{1}{2}\rho v_{rel}^2 \frac{\vec{v_{rel}}}{|\vec{v_{rel}}|} A_{ref} l_F C_F = I\ddot{\theta} \qquad (3)$$

where the produced torque or couple can also be defined by the lift force F_L and associated moment arm l_F.

Assuming that the body of the spacecraft does not contribute any additional roll torques, the lift force coefficient can be recovered by considering the evolution of attitude in the roll-axis of the spacecraft in combination with knowledge of the control inputs, and reaction wheel rates or angular momentum.

Free-parameter fitting of the lift force coefficient from the attitude evolution of the spacecraft requires an attitude dynamics model including models for the torques which act on the spacecraft. The orbit trajectory and perturbation models used in the drag coefficient analysis are also required to provide the correct spatial and temporal reference for the selected torque models.

4. Attitude Stability and Control Analysis

The presence and use of the steerable fins on SOAR produces a number of different forces and torques which need to be carefully considered to ensure stability and pointing accuracy of the spacecraft throughout its lifetime. Interaction of the spacecraft with the residual atmosphere in LEO, solar radiation, and the magnetic and non-spherical gravity fields of the Earth must principally be considered. The capability to control the attitude and stability of the spacecraft using on-board actuators also requires consideration as the orbital altitude decreases and the aerodynamic torques experienced increase in magnitude.

The concept of aerostability is employed by SOAR to provide passive pointing towards the oncoming flow direction in orbit. This aerostability is provided by the steerable fins which are located towards the aft of the spacecraft and thus generate a restoring aerodynamic torque in pitch and/or yaw in response to any misalignment of flow direction with the longitudinal axis of the spacecraft. When each steerable fin is oriented parallel to the longitudinal body axis of the spacecraft a minimum drag configuration is generated for the nominal spacecraft attitude. Similarly, when the steerable fins are all oriented normal to the spacecraft longitudinal axis the maximum drag configuration is achieved.

As the material and surface coatings which will be applied to the steerable fins are yet to be selected for the mission, this creates uncertainty in the attitude performance and control capability of the satellite. Different materials will have varying GSI performance, and may therefore result in the production of significantly different forces and torques when exposed to the flow. In the following analyses Sentman's model [2] for GSIs is used in which the energy accommodation coefficient α and surface (wall) temperature T_w principally govern the quality of particle reflection/reemission.

4.1. Static Stability

The static stability of provided by different configurations of the steerable fins can be investigated by considering the torque generated by the interaction of the spacecraft geometry with the oncoming flow.

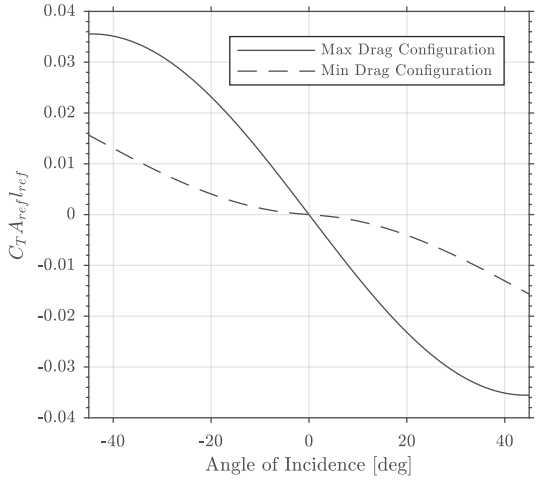

Figure 2: Pitch/Yaw moment coefficient of SOAR with varying angle of incidence with respect to the flow in the minimum (steerable fins parallel to body) and maximum (steerable fins perpendicular to body) drag configurations. Assuming Sentman GSI model at 300 km altitude, 56.1° inclination

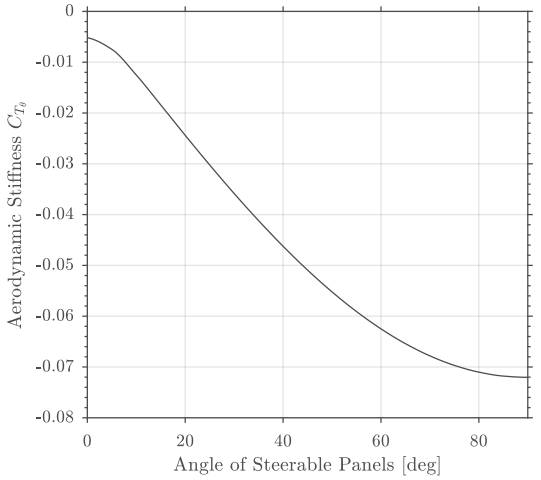

Figure 3: Aerodynamic stiffness, static stability derivative, of SOAR with varying steerable fin angle with respect to the flow. Assuming Sentman GSI model at 200 km altitude, 56.1° inclination

Modelling of the aerodynamic moment coefficients for SOAR has been performed using *ADBSat* [24], an analytical panel-method tool for convex satellite geometries which can encompass different gas-surface interaction models and basic shadowing analysis. In this study Sentman's model is applied throughout with accommodation coefficient $\alpha = 1$ and $T_w = 300$ Kelvin unless otherwise stated.

The static pitching/yawing moment coefficient of SOAR in the minimum and maximum drag configurations is presented in Fig. 2. The negative slope of the pitch/yaw moment coefficient with angle of incidence indicates the aerostable nature of these configurations. The concept of aerodynamic stability derivatives, or aerodynamic stiffness, for spacecraft at orbital altitudes, can be used to further investigate the expected attitude behaviour for varying geometry and flight conditions [25]. The static pitch/yaw stability derivative C_{T_θ}, can be calculated from the gradient of C_T over a small range about the nominal attitude ($\theta = 0$). The variation in static pitch/yaw stability derivative for steerable fin angles over the range of minimum to maximum drag configurations is shown in Fig. 3, noting that the steerable fins are counter-rotated and thus demonstrate symmetry between pitch and yaw. The increase in stability derivative with increasing incidence angle demonstrates that a greater static stability is achieved when a larger panel area is presented to the flow.

In order to characterise the performance of different materials and surface-coatings in orbit, during the experimental periods only one pair of steerable fins will be rotated with respect to the flow at any given time. With this configuration a total of four materials or surfaces can be characterised during the mission, two per pair of opposing steerable fins.

When a single pair of steerable fins is counter-rotated with the spacecraft pointing into the direction of the oncoming flow a net rolling torque is generated but no net pitch or yaw torques are created. However, if the relative direction of the flow changes (for example due to atmospheric co-rotation or thermospheric winds) or the attitude of the satellite is perturbed, induced torques are generated due to a variation in the projected area of the counter-rotated fins to the flow. In Fig. 4 the vertical fins are counter-rotated and the spacecraft attitude is offset with respect to the oncoming flow in sideslip with an angle of 5°. Under these conditions, contrary to either the maximum or minimum drag configurations, a net pitching torque arises due to the difference in area presented to the flow by the vertical fins. The plot of net torques in pitch and yaw for this configuration, shown in Fig. 5, demonstrate that induced torques in pitch due to angle of sideslip have a positive gradient about the equilibrium, and are therefore disturbing rather than restoring. Furthermore, these torques grow at a faster rate than the restoring torques generated by the lateral fins due to pitch angle. If the flow is therefore offset with respect to the spacecraft body in yaw the spacecraft responds by rotating in the pitching axis as a result of the set angle of the steerable fins. Equivalent behaviour is demonstrated for counter-rotated lateral fins and an offset in angle of attack. This effect is therefore termed pitch-yaw coupling henceforth.

Co-rotation of a pair of opposing steerable fins generates a net torque in pitch or yaw, but no net torque in roll. Fig. 5 shows the torques in pitch and yaw for a configuration in which the lateral fins are co-rotated, demonstrating a small bias in pitch torque when the spacecraft is aligned with the direction of the oncoming flow. However, as the pitch (angle of attack) is increased by a small amount ($\sim 3°$ in Fig. 5) the pitch torque crosses zero with a negative gradient. The spacecraft therefore demonstrates stability in

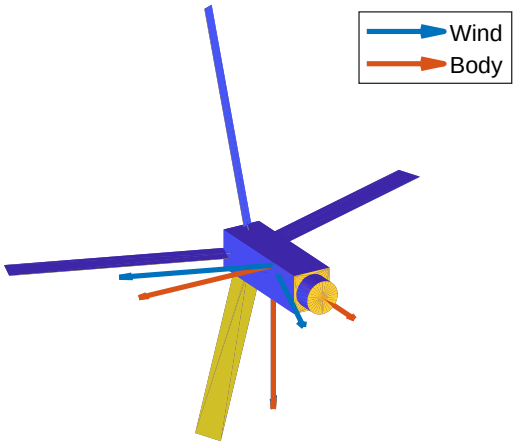

Figure 4: SOAR geometry with vertical fins counter-rotated at 45°. The 5° sideslip angle of the flow produces a variation in projected area between the vertical fins and results in a disturbing pitch torque.

pitch at this small angle with respect to the flow. The spacecraft is also shown to be stable in yaw about the oncoming flow direction.

4.2. Dynamic Stability

In order to understand the evolution of attitude over time and in the presence of perturbing torques the dynamic response of the spacecraft must be considered. For rotationally symmetric configurations the previous analyses showed that aerostability ensures that restoring torques will be produced in response to changes in the oncoming flow direction. However, due to the FMF nature of the surrounding atmospheric environment, natural damping of the generated angular velocity is not generated. Therefore, without any additional damping input or further perturbation to the system, the spacecraft will oscillate about an equilibrium point. The amplitude and frequency of this oscillation are dependant on the initial disturbance, stability derivative, and the environmental conditions Mostaza-Prieto and Roberts [25].

The response of SOAR in the minimum and maximum drag configuration for varying orbital altitude and in the absence of further perturbing torques is presented in Fig. 7. The responses demonstrate the aerostable nature of the spacecraft configuration and that the amplitude and period of oscillation both decrease with increasing aerodynamic stiffness and dynamic pressure.

This oscillatory mode can be critically damped, significantly reducing the range over which the attitude of the spacecraft varies, as discussed by Virgili Llop et al. [26]. However, due to the presence of further perturbing torques in the real orbital environment (eg. thermospheric winds, solar-radiation pressure, gravity gradient), and errors or incompatibilities associated with real attitude actuator systems (eg. magnetorquer availability and cross-coupling), the true dynamic response is more complex.

Further control methods for aerostable spacecraft are presented in the literature, but have not yet been tested beyond simulation. Psiaki [27] presents a compass-like PID control method which utilises magnetorquers to provide three-axis stabilised nadir-pointing capability to a 1U CubeSat with a shuttlecock configuration of deployed 'feathers'. Auret and Steyn [28] subsequently applied this method to an extended 3U CubeSat geometry which included a pair of actuating 'paddles', provide control capability about the roll axis. Further control methods utilising reaction wheels were also investigated, including a 3-axis quaternion feedback control law providing pointing performance for imaging applications.

A further issue with active control of a flow-pointing spacecraft is that the true oncoming flow vector is not known a priori. A reference vector for true three-axis flow-pointing control using proportional control inputs is therefore missing. A predicted vector can be used including the effect of atmospheric co-rotation, however the integration of thermospheric winds using available models is associated with much greater uncertainty.

5. Mission Simulations

The orbit and attitude response of SOAR in the VLEO environment can be investigated a 6-DOF orbital propagator, simulating periods of the planned mission. In these simulations this tool incorporates the forces and torques associated with the Earth gravitational potential (analytical J_4 or EGM2008 [29]), solar radiation pressure, residual magnetic dipole interactions (IGRF-11 [30]), varying atmospheric density (NRLMSISE-00 [31]), and thermospheric winds (HWM93 [32] and HWM07 [33]).

As above, the ADBSat tool [24] is used to calculate altitude-dependent aerodynamic coefficients using Sentman's GSI model. However, it is important to recall that the results presented herein will be subject to the assumptions and limitations of the implemented GSI model and the input parameters used and therefore may differ substantially from the true behaviour in orbit.

Control of the spacecraft in these simulations is provided by modelled reaction wheel actuators which are configured in a tetrahedral formation providing redundancy and a dedicated wheel in the roll-axis. The inputs to the reaction wheels are provided by a proportional-derivative controller (without knowledge of the true oncoming flow direction). The implemented control gains are currently set empirically as the development of other control methods, including adaptive and optimal control, will be explored in future work. Desaturation of the reaction wheels will be performed if necessary during the idle operations and between experimental test-runs using the magnetorquer actuators.

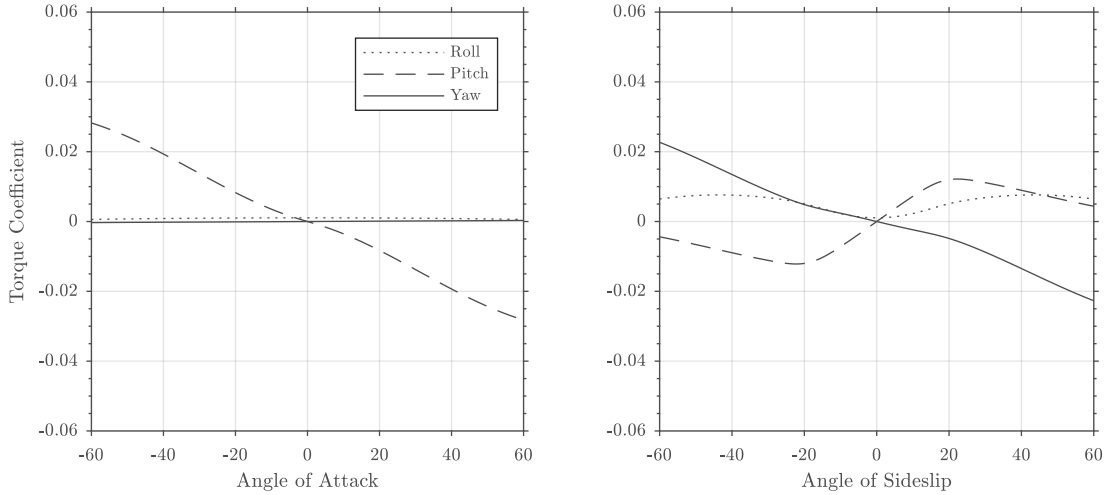

Figure 5: Pitch-Yaw coefficient response for SOAR with vertical fins counter-rotated at incidence angle of 20°

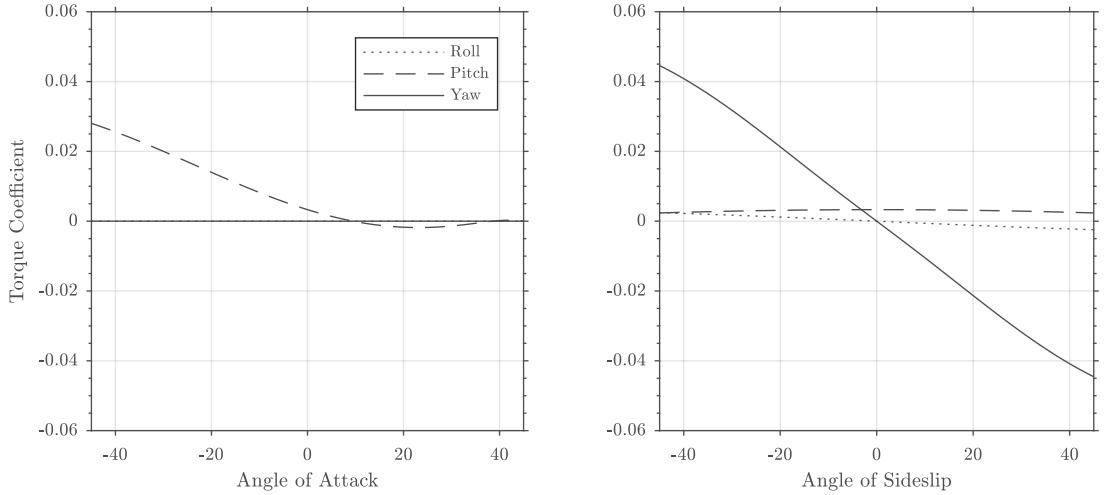

Figure 6: Pitch-Yaw coefficient response for SOAR with lateral fins co-rotated at incidence angle of 20°

5.1. Idle Operations

At the beginning of the mission SOAR will be deployed from the ISS to an altitude of approximately 400 km approximately 400 km. As this deployment is expected to be Q1 2020, expected to be the beginning of a very low activity solar minimum, the atmospheric density at this altitude will extremely low compared to later in the mission lifecycle and aerodynamic torques experienced by the spacecraft will be relatively small in comparison to the expected solar radiation pressure, residual magnetic dipole, and gravity gradient torques. The natural attitude response of SOAR without any active actuation under these conditions is shown in Fig. 8, indicating flow-pointing angular errors generally within ±30° in pitch and yaw when in the minimum-drag condition. The maximum drag configuration is shown to reduce the amplitude of oscillation by increasing the aerodynamic stiffness of the satellite, resulting in flow-pointing angular errors within ±10° for the same conditions. Fig. 8 also shows that a greater energy accommodation coefficient slightly increases the attitude angle range experienced by SOAR in these configurations, demonstrating the effect that different materials or surface-coatings can have on the attitude dynamics of the spacecraft.

The results of these simulations suggest that it may be necessary at the beginning of the mission (assuming an insertion altitude of 400 km and low solar activity conditions) to increase the stability of the satellite by operating in the maximum drag configuration, albeit at the expense of total orbital lifetime. As the satellite descends in altitude the atmospheric density will increase and aerostability in the the minimum drag configuration will improve such that it can be utilised whilst maintaining small flow-pointing angular errors.

The active attitude actuators (reaction wheels and magnetorquers) on SOAR can be used to further reduce the oscillatory motion of SOAR and provide finer flow-pointing attitude. However, as the perturbing torques are not all periodic in nature, in particular those due to solar radiation pressure, the angular momentum of the reaction

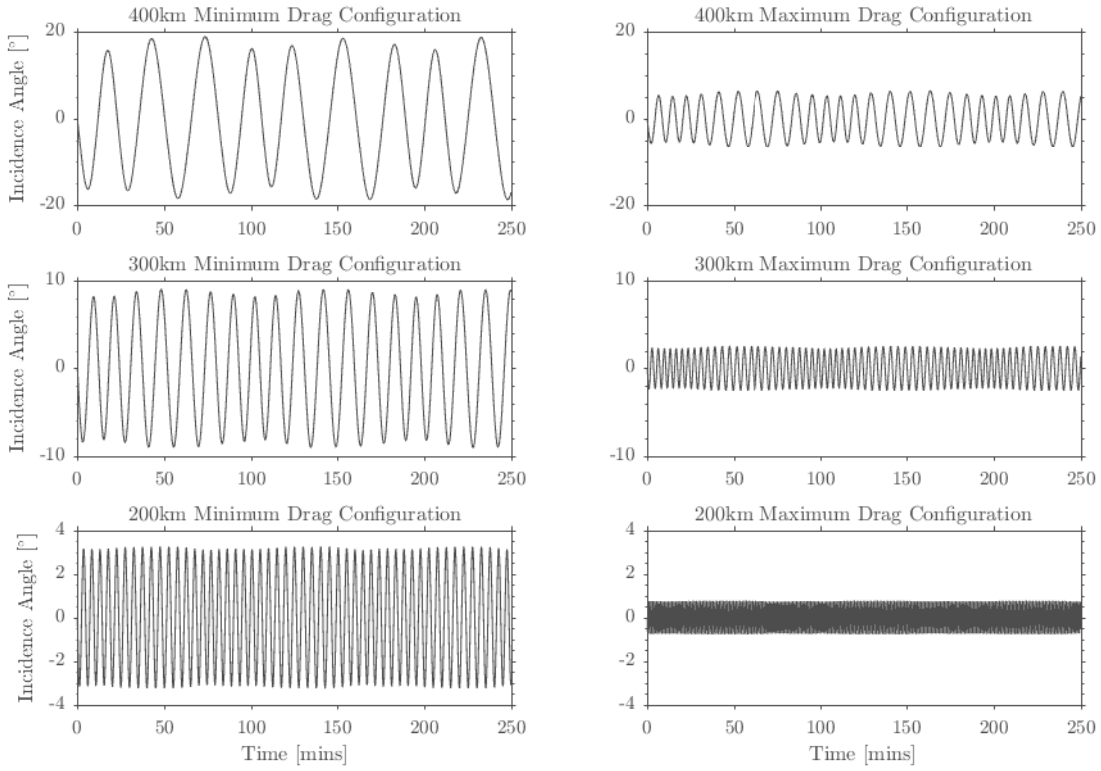

Figure 7: Uncontrolled and aerostable pitch/yaw attitude response of SOAR geometry for varying altitude and steerable fin configuration. Attitude simulation performed considering only aerodynamic torques in an equatorial orbit.

wheels requires management in order to avoid saturation. Furthermore, the typical disadvantages of cross-coupling and limited availability of magnetorquers must also be accommodated whilst the the power consumption of the actuators must be considered for extended use and through eclipse periods.

5.2. Experimental Operations

During the experimental operation of SOAR, both the co-rotated and counter-rotated configurations of the steerable fins can be considered.

In the counter-rotated configuration the spacecraft is nominally pointed towards the oncoming flow direction as no torques are in generated in pitch or yaw. A net torque in roll is however produced, which if uncontrolled will cause the spacecraft to spin up. As a result of natural aerostability, oscillations in the pitch and/or yaw attitude will be produced when the spacecraft is disturbed from its equilibrium flow pointing configuration. The effect of pitch-yaw coupling will then also act to disturb the attitude of the spacecraft from the flow-pointing direction.

During drag coefficient experiments, the attitude will be controlled in three axes avoiding roll-up of the spacecraft. Contrastingly, two alternative methods for the investigation of the lift-force coefficient are proposed. The first can be performed alongside the experiments on the drag-coefficient under three-axis attitude control and utilises the principal of conservation of momentum between the reaction wheels and the spacecraft body to recover the aerodynamic torque in the roll axis and therefore the coefficient of lift-force. The second allows the roll axis to remain uncontrolled allowing the acceleration in roll to be measured by the attitude-determination system.

Control of the roll torque and pitch-yaw coupling effects causes build-up in the angular momentum in the reaction wheels towards saturation. Similar to the previous analyses, these effects are strongly linked to the atmospheric density or dynamic pressure. However, as the density increases the magnitude of the pitch-yaw coupling and roll torques also increase and the spacecraft becomes more difficult to control with the attitude actuators. However, in general the counter-rotated configuration ensures that the INMS device is pointed towards and oscillates across the oncoming flow direction and can be operated within its angular acceptance range. The counter-rotated mode is therefore preferable for the use of the INMS to measure the in-situ atmospheric density and flow velocity successfully during the experimental periods.

In the alternative co-rotated configuration, pitch or yaw torques are generated by the common incidence angle of the two opposing steerable fins, causing the spacecraft to fly at an angle to the oncoming flow. This behaviour is also associated with an oscillatory motion about an equilibrium attitude, resulting from the aerostability of the spacecraft. However, as the nominal attitude of the satellite will be biased in either pitch or yaw, control actuators must be

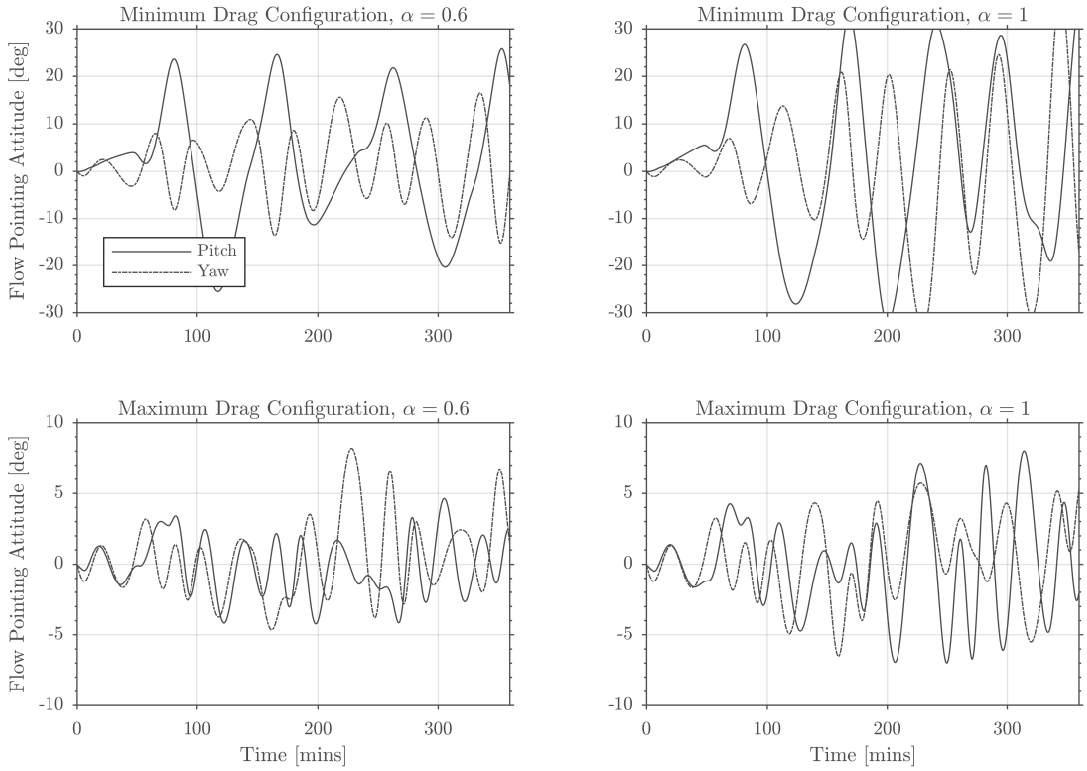

Figure 8: Nominal uncontrolled attitude response of SOAR in the minimum drag and maximum drag configuration with two different accommodation coefficients $\alpha = 0.6$ and $\alpha = 1$ at 400 km altitude and under low solar activity conditions. Aerodynamic coefficients calculated using ADBSat and Sentman's model with $T_w = 300\,\mathrm{K}$.

used to correct the nominal pointing direction such that the INMS will be aligned towards the flow, ensuring the accuracy of the measured density and flow velocity information. As a bias in the pitch or yaw torques exists, angular momentum will build-up in the reaction wheels and eventually cause saturation of the control system.

5.2.1. Three-axis Attitude Control

The response of SOAR under three-axis attitude control with one set of steerable fins counter-rotated at an angle of 45° is shown in Fig. 9 for two different altitudes. At the lower altitude of 250 km the limit of the reaction wheel assembly is reached as the rates increase to saturation after 20 min. This results in a loss of control actuation and subsequent roll-up of the satellite. The magnitude of the pitch and yaw oscillations of the spacecraft also begin increase to above 20°, beyond the acceptance range of the INMS.

At the higher altitude of 350 km attitude control can be sustained by the reaction wheels for a much longer period with less build-up of angular momentum, a product of the lower density atmosphere and therefore aerodynamic torques of smaller magnitude. The attitude in pitch and yaw of the spacecraft is also shown to be maintained within a much smaller angular range (<45°) and within the acceptance angle range of the INMS, thereby enabling direct measurement of the in-situ density throughout the experimental period.

Practically, a maximum duration on operations with fins angled in a counter-rotated configuration is imposed by the build-up of angular momentum in the reaction wheels which exists as a factor of the atmospheric density, incidence angle of the steerable fins, and material performance. The thermospheric wind and solar activity also contribute to this attitude performance, but vary with much greater uncertainty. At lower altitudes the time-period over which spacecraft can be operated successfully may therefore be significantly limited for some experimental configurations, the impact of which will be discussed later in Section 6 with regards to the experimental uncertainty.

The corresponding behaviour for the co-rotated configuration under three-axis control is shown in Fig. 10. In this configuration the satellite similarly suffers saturation of the reaction wheels after only a short period at the 250 km altitude. However, an offset in yaw attitude from the oncoming flow direction is also initially presented as a result of the torque bias generated by the co-rotated vertical fins. Furthermore, the oscillations associated with this motion do not regularly cross the oncoming flow direction. This poses an issue with the simultaneous operation of the INMS during the experimental test runs as a bias in the density measurement associated with the angular offset from the flow direction may be present. At 350 km altitude the attitude of the spacecraft in all three axes is generally controlled to within ±5° and without saturating the reaction wheels.

5.2.2. Pitch and Yaw Control

SOAR can also be operated in a two-axis control mode in which the roll-axis is left uncontrolled, allowing the torques in this axis to be measured without direct contribution from the z-axis wheel. With a counter-rotated configuration of the steerable fins the spacecraft is expected to immediately spin-up in roll due to the production of equal but opposite side-forces and thus a net-torque by the steerable fin pair. The response of SOAR under two-axis (pitch and yaw only) attitude control with one set of steerable fins counter-rotated at an angle of 45° is shown in Fig. 11.

At both 250 km and 350 km altitudes, the spacecraft expectedly starts to roll as a result of the counter-rotated fin configuration. Differences are shown in the rate at which the spacecraft angular velocity increases in the roll axis and the angular range simultaneously experienced in the pitch and yaw axes, as a result of the density variation at the two altitudes. Similarly to previous analyses, control in the pitch and yaw axes results in reaction wheel saturation at the lower altitude, whilst control can be maintained for a longer period at the higher altitude.

The attitude response with pitch and yaw control for co-rotated configurations is shown in Fig. 12. At 250 km altitude, similarly to the case of three axis control, the yaw motion is shown to oscillate at an offset from the flow pointing direction. The angular errors in pitch and yaw are also of a similar magnitude and the reaction wheels quickly become saturated. At 350 km altitude, the angular errors are shown to be slightly greater under the pitch-yaw only control, approaching ±10° at towards the end of the analysed period.

In both the counter-rotated and co-rotated configurations the attitude evolution in roll is also shown to vary as a result of gyroscopic precession effects and the angular momentum distribution in the reaction wheel assembly, resulting at times in the reversal of the roll-rate.

6. Experimental Uncertainty

The expected performance of the mission and the experimental determination of the aerodynamic coefficients can be investigated by testing the free-parameter fitting and least-squares processes using simulated orbit and attitude data. This data can also be further modified with additional noise to represent the expected sensor performance. A Monte Carlo approach is implemented to encompass variation in the initial conditions (epoch, orbit, and attitude) and randomise the addition of noise to the data for each simulated run.

The simulated attitude and orbit data is produced using the orbit propagation method described previously in Section 5. Orbit and attitude noise is produced by considering the performance parameters of the GPS and ADCS sensors, reported in Table 1. Uncertainty on the angular position of the steerable fins is also introduced based on the expected precision of the rotary encoder.

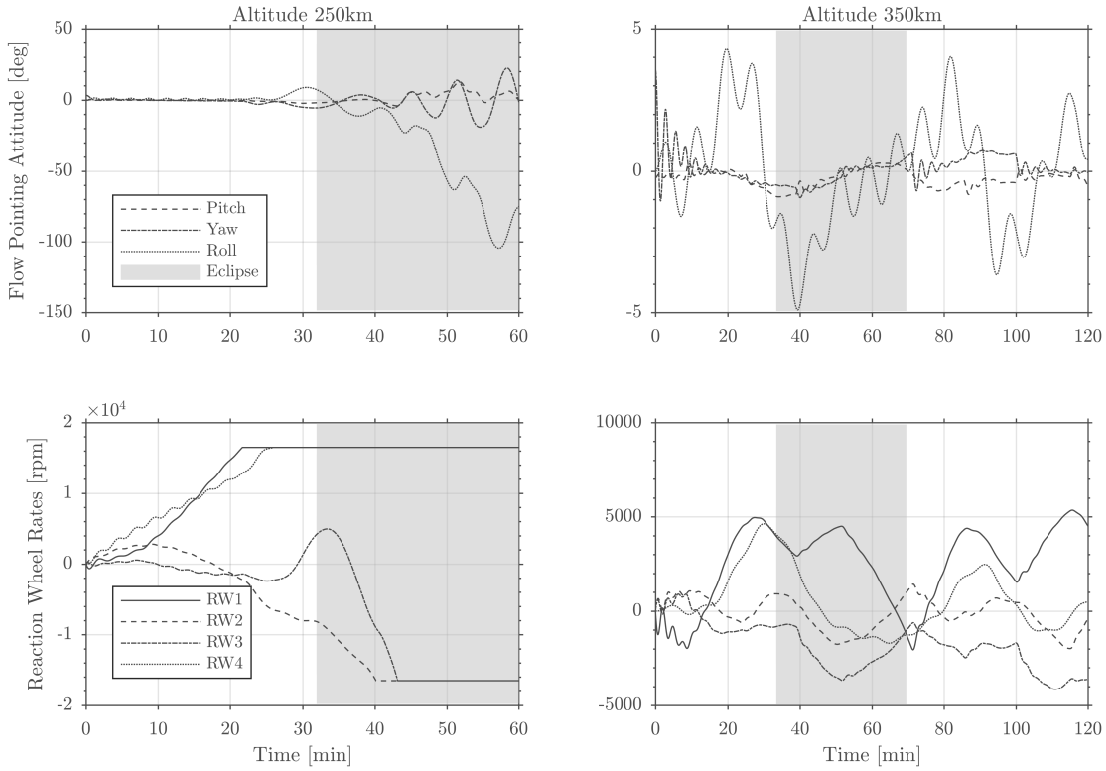

Figure 9: Attitude response of SOAR at 250 km and 350 km altitude with vertical steerable panels counter-rotated at 45° and three-axis reaction wheel control under low solar activity conditions. Aerodynamic coefficients calculated using ADBSat and Sentman's model with $\sigma = 1$ and $T_w = 300\,\mathrm{K}$.

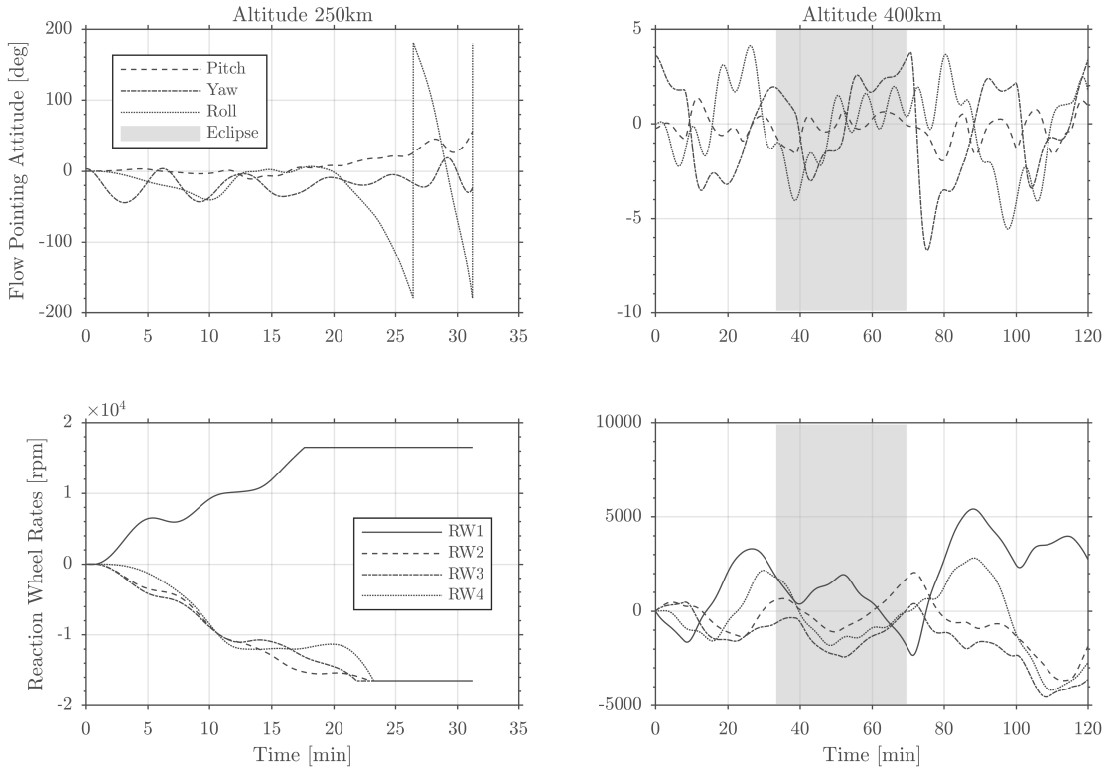

Figure 10: Attitude response of SOAR at 250 km and 350 km altitude with vertical steerable panels co-rotated at 45° and three-axis reaction wheel control under low solar activity conditions. Aerodynamic coefficients calculated using ADBSat and Sentman's model with $\sigma = 1$ and $T_w = 300\,\mathrm{K}$.

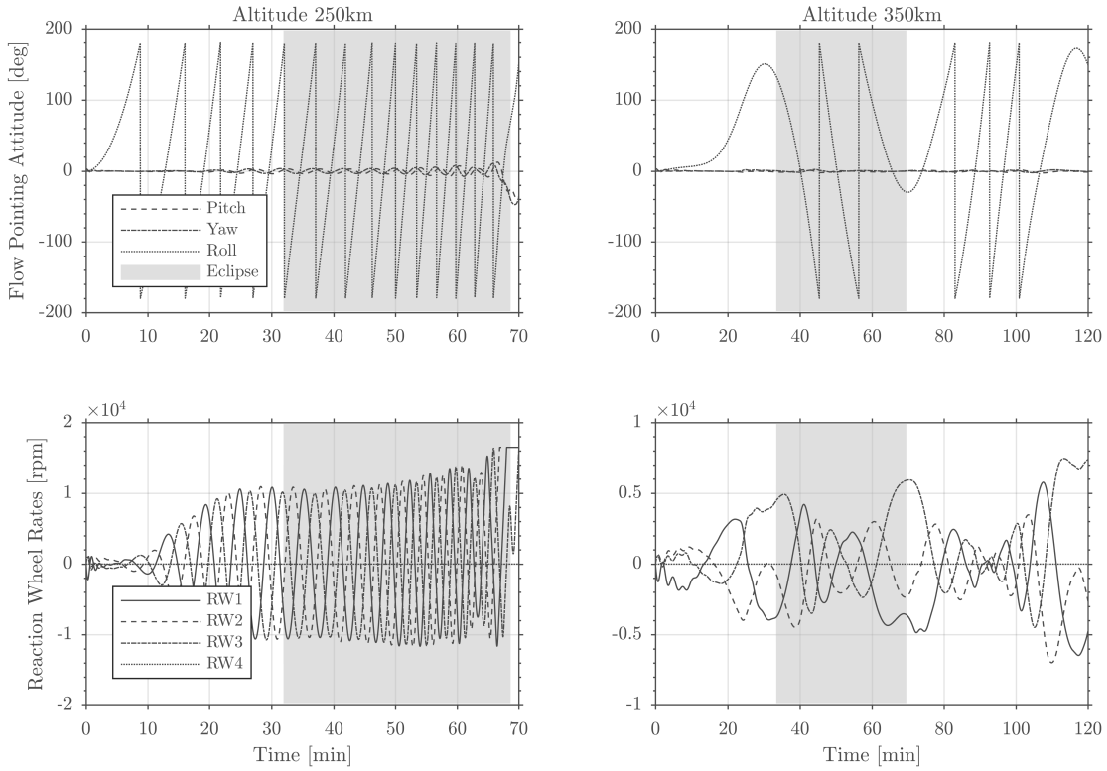

Figure 11: Attitude response of SOAR at 250 km and 350 km altitude with vertical steerable panels counter-rotated at 45° and pitch-yaw reaction wheel control under low solar activity conditions. Aerodynamic coefficients calculated using ADBSat and Sentman's model with $\sigma = 1$ and $T_w = 300\,\mathrm{K}$.

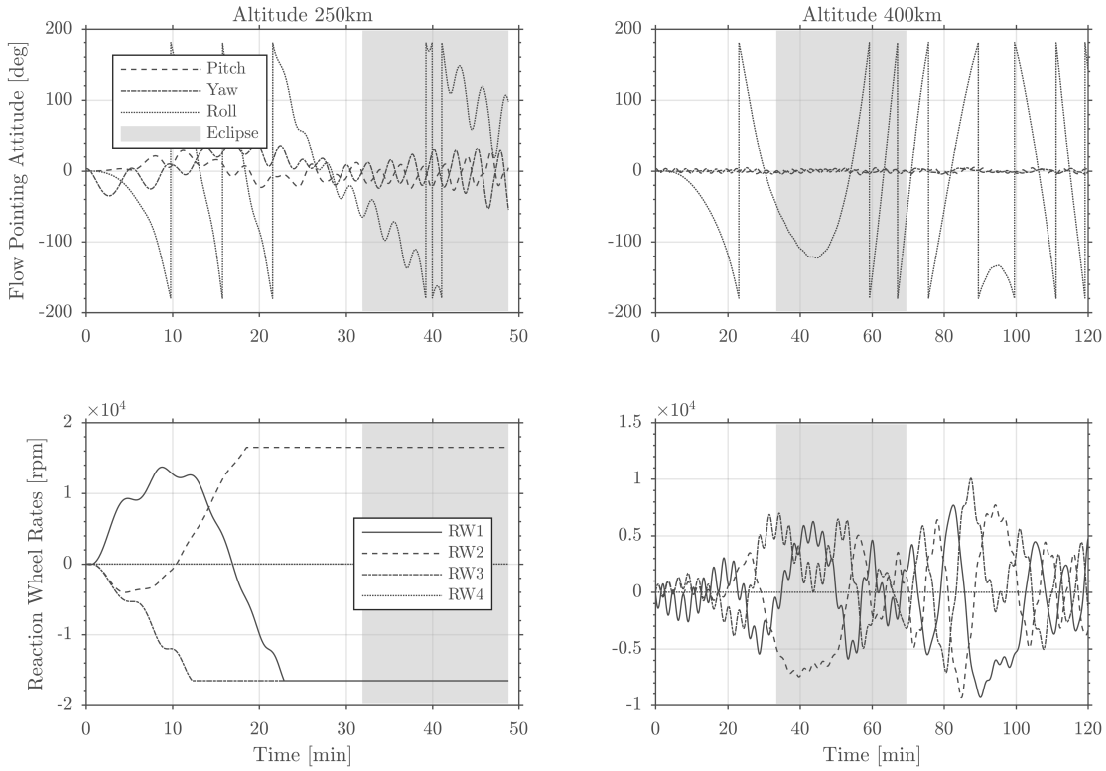

Figure 12: Attitude response of SOAR at 250 km and 350 km altitude with vertical steerable panels co-rotated at 45° and pitch-yaw reaction wheel control under low solar activity conditions. Aerodynamic coefficients calculated using ADBSat and Sentman's model with $\sigma = 1$ and $T_w = 300\,\mathrm{K}$.

The performance and data output of the the INMS is simulated prior to use in the free parameter fitting process. The measured density is first produced using the NRLMSISE-00 [31] atmosphere model, informed by orbit and attitude data previously modified for GPS and ADCS sensor and acquisition errors and noise. This density is then subsequently transformed using the INMS instrument uncertainty, also reported in Table 1. Finally, data points for which the spacecraft would be pointing outside the angular acceptance range of the INMS are rejected and the missing values replaced by interpolation between neighbouring valid data-points.

The free-parameter fitting process utilises a least-squares orbit determination algorithm which seeks to minimise the error between the reference and modelled trajectories by varying the *free* values of the aerodynamic coefficients. This process is iterative and is terminated by convergence criteria. Finite- or central-differencing methods are used to account for the errors in the initial condition of the state vector.

The expected experimental performance at different orbital altitudes and steerable-fin configurations can be obtained by considering the standard deviation or confidence interval of the returned aerodynamic coefficient after a number of Monte Carlo iterations. Overlap in the standard deviation for two configurations suggests that the difference in fitted drag coefficient for these two results may not be statistically significant and therefore may not identifiable from each other in the current experiment. The impact of the use of the Monte Carlo simulations can also be investigated by considering the confidence interval on the fitted drag coefficient or the standard deviation.

Reducing this standard deviation, effectively the resolution of the experiment, can be achieved by increasing the signal-to-noise ratio, for example by increasing the test run time or reducing the uncertainties associated with the utilised data.

Table 1: Summary of expected satellite sensor performance.

Instrument	1σ **Uncertainty**
GPS Position [m]	2.5
GPS Velocity [$\mathrm{m\,s^{-1}}$]	45×10^{-3}
ADCS Angle [rad]	0.2×10^{-3}
ADCS Angular Velocity [$\mathrm{rad\,s^{-1}}$]	25×10^{-3}
INMS Number Density [$\mathrm{cm^{-3}}$]	$\sqrt{\rho_N} + 0.7$
Steerable Fin Rotation Angle [rad]	0.0175

Fig. 13 shows the returned drag coefficients from this data reduction process for SOAR operating with a range of different steerable-fin (counter-rotated) incidence angles and at several altitudes below 400 km. For these drag-coefficient experiments an experimental period of 120 min is targeted, encompassing more than a single orbital period, and three-axis reaction wheel attitude control is implemented. The test-run is aborted if the angular range in pitch or yaw exceeds the INMS acceptance limit of 10° or the reaction wheels approach 90 % saturation. Reference lines for the GSI-based drag coefficient at each altitude and configuration have been provided.

These results indicate that experimentally determined drag coefficients for the different steerable fin incidence angles are likely to be identifiable and distinguishable within altitude range of 250 km to 350 km, with the exception of high-incidence angles (60° to 90°) at 350 km. Above and below this altitude range the expected uncertainty is much greater and the experimentally determined drag coefficients many not be distinguishable from other configurations. Variation in the experimentally determined results and the reference (GSI-based) drag-coefficients arise primarily from the variation in cross-sectional area and steerable fin incidence angle which occurs as the satellite oscillates in pitch and yaw. Additional sources of error can be attributed to the sensor characteristics and noise parameters and the least-squares fitting process.

The variation of the drag coefficient with altitude for each steerable fin configuration also does not appear to be identifiable from the expected experimental performance. This is due to the relatively small variation in drag coefficient which is expected over the available altitude range and the experimental uncertainties arising from the spacecraft dynamics and sensor characteristics. However, Sentman's GSI model with a single accommodation coefficient ($\sigma = 1$) has been used to generate these results and they are therefore subject to the inherent assumptions and simplifications of the model. These results are also therefore not representative of the different materials which will be used to cover the steerable fin surfaces. Significantly, these materials may demonstrate variation in atomic oxygen accommodation with orbital altitude which would increase the corresponding drag coefficient.

The corresponding standard deviation of the drag coefficient is shown in Fig. 14. These results indicate that the experimental uncertainty first decreases with reducing altitude. This is a result of the increasing atmospheric density and therefore greater aerodynamic forces which generate a variation in the trajectory that can be identified against the noise in the measured parameters. The 200 km and 225 km altitude runs with non-minimum or maximum drag configurations also show significantly higher uncertainty. This results from very short experimental runs (average of 17.8 min) as the spacecraft dynamics at the low altitude and higher atmospheric density cause the reaction wheels to saturate quickly. However, at these altitudes the lifetime will be very short and it is not expected that drag coefficient experiments will principally performed in this range.

7. Concluding Remarks

The simulated dynamics of the SOAR spacecraft demonstrate the aerostable nature of the design and the capabil-

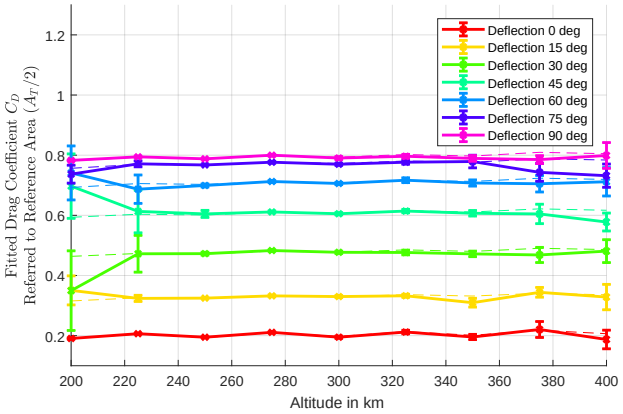

Figure 13: Simulated fitted drag coefficient for varying steerable-fin counter-rotation angle and altitude. Error-bars represent the expected 95 % confidence interval on the fitted drag coefficient calculated from a 25 sample Monte Carlo simulation.

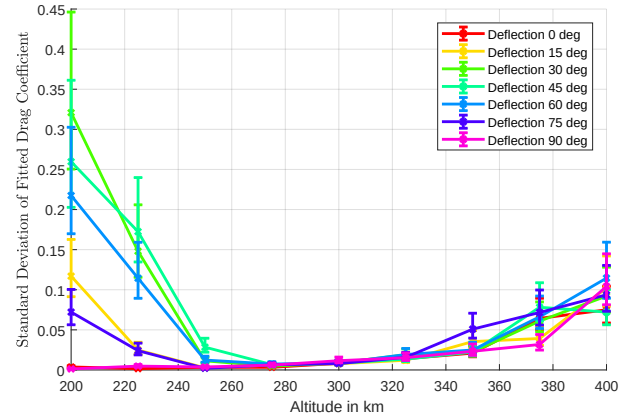

Figure 14: Expected standard deviation of simulated fitted drag coefficient for varying steerable-fin counter-rotation angle and altitude. Error-bars represent the 95% confidence interval on this standard deviation calculated from 25 sample Monte Carlo simulation.

ity to operate successfully with the steerable-fins in both counter-rotated and co-rotated modes over a range of orbital altitudes in VLEO.

The combination of the INMS and steerable fin payloads are shown to enable experimental assessment of the drag coefficient of different materials exposed to the flow at varying incidence and over a range of altitudes as the spacecraft descends due to orbital decay. Methods for the recovery of the lift coefficient have also been proposed but require further mission analysis.

Simulations of the expected experimental performance demonstrate constraints on both the maximum and minimum altitudes at which the drag coefficient for different configurations can be successfully recovered from the measured orbital parameters. At high altitudes longer test runs or larger steerable fins are be required to improve the experimental uncertainty due to the expected noise associated with the GPS position and velocity measurements. At lower altitudes saturation of the reaction wheels can significantly limit the experimental period.

Implementation of more complex attitude control methods, for example using adaptive or model-predicted methods, may be able to extend the capabilities of the reaction wheels and therefore the experimental uncertainty at lower altitudes. However, uncertainty and variability in the oncoming flow direction will remain a challenge. Active tracking of the flow direction by the steerable fins could also be utilised to reduce the variation in cross-sectional area and therefore also improve the experimental performance.

Acknowledgements

The DISCOVERER project has received funding from the European Union's Horizon 2020 research and innovation programme under grant agreement No 737183.

References

References

[1] P. C. Roberts, N. H. Crisp, S. Edmondson, S. J. Haigh, R. E. Lyons, V. T. Oiko, A. Macario-Rojas, K. L. Smith, J. Becedas, G. González, I. Vázquez, Á. Braña, K. Antonini, K. Bay, L. Ghizoni, V. Jungnell, J. Morsbøl, T. Binder, A. Boxberger, G. Herdrich, F. Romano, S. Fasoulas, D. Garcia-Almiñana, S. Rodriguez-Donaire, D. Kataria, M. Davidson, R. Outlaw, B. Belkouchi, A. Conte, J. S. Perez, R. Villain, B. Heißerer, A. Schwalber, DISCOVERER – Radical Redesign of Earth Observation Satellites for Sustained Operation at Significantly Lower Altitudes, in: 68th International Astronautical Congress, September, International Astronautical Federation (IAF), Adelaide, Australia, 2017.

[2] L. H. Sentman, Free molecule flow theory and its application to the determination of aerodynamic forces, Tech. Rep., Lockheed Missiles & Space Company, Sunnyvale, CA, 1961.

[3] D. Mostaza-Prieto, B. P. Graziano, P. C. Roberts, Spacecraft drag modelling, Progress in Aerospace Sciences 64 (2014) 56–65, ISSN 03760421, doi:10.1016/j.paerosci.2013.09.001, URL `http://dx.doi.org/10.1016/j.paerosci.2013.09.001`.

[4] K. Moe, M. M. Moe, S. D. Wallace, Improved Satellite Drag Coefficient Calculations from Orbital Measurements of Energy Accommodation, Journal of Spacecraft and Rockets 35 (3) (1998) 266–272, ISSN 0022-4650, doi:10.2514/2.3350, URL `http://arc.aiaa.org/doi/10.2514/2.3350`.

[5] B. R. Bowman, K. Moe, Drag Coefficient Variability at 175-500km from the Orbit Decay Analyses of Spheres, in: AAS/AIAA Astrodynamics Specialists Conference, American Astronautical Society (AAS), Lake Tahoe, CA, 2005.

[6] E. K. Sutton, Normalized Force Coefficients for Satellites with Elongated Shapes, Journal of Spacecraft and Rockets 46 (1) (2009) 112–116, ISSN 0022-4650, doi:10.2514/1.40940, URL `http://arc.aiaa.org/doi/10.2514/1.40940`.

[7] S. A. Schaaf, P. L. Chambre, Flow of rarefied gases, in: Fundamental of Gas Dynamics, vol. III, chap. Section H, Princeton University Press, Princeton, NJ, ISBN 0691625700, 687–739, 1958.

[8] R. Schamberg, A New Analytic Representation of Surface Interaction for Hyperthermal Free Molecule Flow with Applications to Neutral-particle Drag Estimates of Satellites, Research memorandum, Rand Corporation, 1959.

[9] E. M. Gaposchkin, Calculation of Satellite Drag Coefficients, Technical Report 998, Lincoln Laboratory, MIT, Lexington, MA, 1994.

[10] J. Storch, Aerodynamic Disturbances on Spacecraft in Free-Molecular Flow, TR-2003(3397)-1, The Aerospace Corporation, El Segundo, CA, 2002.

[11] K. Moe, M. M. Moe, Gas-Surface Interactions in Low-Earth Orbit, in: 27th International Symposium on Rarefied Gas Dynamics, AIP Conference Proceedings, vol. 1333, American Institute of Physics, Pacific Grove, CA, ISBN 9780735408890, ISSN 0094243X, 1313–1318, doi:10.1063/1.3562825, URL http://aip.scitation.org/doi/abs/10.1063/1.3562825, 2011.

[12] M. D. Pilinski, Dynamic Gas-Surface Interaction Modeling for Satellite Aerodynamic Computations, Phd thesis, University of Colorado, 2011.

[13] A. Hedin, B. Hinton, G. Schmitt, Role of Gas-Surface Interactions in the Reduction of Ogo 6 Neutral Particle Mass Spectrometer Data, Journal of Geophysical Research 78 (22) (1973) 4651–4668, ISSN 01480227, doi:10.1029/JA078i022p04651, URL http://doi.wiley.com/10.1029/JA078i022p04651.

[14] J. Gregory, P. Peters, A Measurement of the Angular Distribution of 5eV Atomic Oxygen Scattered off a Solid Surface in Earth Orbit, Rarefied Gas Dynamics 15 (1).

[15] G. Karr, J. Gregory, P. Peters, Free Molecule Lift and Drag deduced from Shuttle Flight Experiment, Rarefied Gas Dynamics 15 (1).

[16] R. C. Blanchard, Rarefied Flow Lift-to-Drag Measurements of the Shuttle Orbiter, in: 15th ICAS Congress, American Institute of Aeronautics and Astronautics (AIAA), London, 1986.

[17] R. C. Blanchard, J. Y. Nicholson, Orbiter Rarefied-Flow Reentry Measurements from the OARE on STS-62, TM-110182, NASA, Hampton, VA, 1995.

[18] K. Moe, Absolute Atmospheric Densities Determined from the Spin and Orbital Decays of Explorer VI, Planetary and Space Science 14 (11) (1966) 1065–1075, ISSN 00320633, doi:10.1016/0032-0633(66)90022-5.

[19] K. Moe, B. R. Bowman, The Effects of Surface Composition and Treatment on Drag Coefficient of Spherical Satellites, in: AAS/AIAA Astrodynamics Specialists Conference, American Astronautical Society (AAS), Lake Tahoe, CA, ISBN 087703527X, ISSN 00653438, 2005.

[20] B. Ching, D. Hickman, J. Straus, Effects of atmospheric winds and aerodynamic lift on the inclination of the orbit of the S3-1 satellite, Journal of Geophysical Research 82 (10) (1977) 1474–1480, ISSN 01480227, doi:10.1029/JA082i010p01474, URL http://doi.wiley.com/10.1029/JA082i010p01474.

[21] C. Pardini, L. Anselmo, K. Moe, M. M. Moe, Drag and energy accommodation coefficients during sunspot maximum, Advances in Space Research 45 (5) (2010) 638–650, ISSN 02731177, doi:10.1016/j.asr.2009.08.034, URL http://dx.doi.org/10.1016/j.asr.2009.08.034.

[22] A. Macario-Rojas, K. Smith, N. Crisp, P. Roberts, Atmospheric interaction with nanosatellites from observed orbital decay, Advances in Space Research 61 (12) (2018) 2972–2982, ISSN 02731177, doi:10.1016/j.asr.2018.02.022.

[23] J. Virgili Llop, P. C. Roberts, ΔDsat, a QB50 CubeSat mission to study rarefied-gas drag modelling, Acta Astronautica 89 (2013) 130–138, ISSN 00945765, doi:10.1016/j.actaastro.2013.04.006, URL http://dx.doi.org/10.1016/j.actaastro.2013.04.006.

[24] D. Mostaza-Prieto, Characterisation and Applications of Aerodynamic Torques on Satellites, Phd thesis, The University of Manchester, 2017.

[25] D. Mostaza-Prieto, P. C. Roberts, Methodology to Analyze Attitude Stability of Satellites Subjected to Aerodynamic Torques, Journal of Guidance, Control, and Dynamics 39 (3) (2016) 437–449, ISSN 0731-5090, doi:10.2514/1.G001481, URL http://arc.aiaa.org/doi/10.2514/1.G001481.

[26] J. Virgili Llop, P. C. Roberts, Z. Hao, Aerodynamic Attitude and Orbit Control Capabilities of The ΔDsat CubeSat, in: 37th Annual AAS Guidance and Control Conference, AAS 14-063, American Astronautical Society (AAS), Breckenridge, CO, 2014.

[27] M. L. Psiaki, Nanosatellite Attitude Stabilization Using Passive Aerodynamics and Active Magnetic Torquing, Journal of Guidance, Control, and Dynamics 27 (3) (2004) 347–355, ISSN 0731-5090, doi:10.2514/1.1993, URL http://arc.aiaa.org/doi/10.2514/1.1993.

[28] J. Auret, W. H. Steyn, Design of an Aerodynamic Attitude Control System for a Cubesat, 62nd International Astronautical Congress .

[29] N. K. Pavlis, S. A. Holmes, S. C. Kenyon, J. K. Factor, The development and evaluation of the Earth Gravitational Model 2008 (EGM2008), Journal of Geophysical Research: Solid Earth 117 (B4), ISSN 01480227, doi:10.1029/2011JB008916, URL http://doi.wiley.com/10.1029/2011JB008916.

[30] C. C. Finlay, S. Maus, C. Beggan, T. Bondar, A. Chambodut, T. Chernova, A. Chulliat, V. Golovkov, B. Hamilton, M. Hamoudi, R. Holme, G. Hulot, W. Kuang, B. Langlais, V. Lesur, F. Lowes, H. Lühr, S. Macmillan, M. Mandea, S. McLean, C. Manoj, M. Menvielle, I. Michaelis, N. Olsen, J. Rauberg, M. Rother, T. Sabaka, A. Tangborn, L. Tøffner-Clausen, E. Thébault, A. Thomson, I. Wardinski, Z. Wei, T. Zvereva, International Geomagnetic Reference Field: The eleventh generation, Geophysical Journal International 183 (3) (2010) 1216–1230, ISSN 0956540X, doi:10.1111/j.1365-246X.2010.04804.x.

[31] J. Picone, A. Hedin, D. P. Drob, A. Aikin, NRLMSISE-00 Empirical Model of the Atmosphere: Statistical Comparisons and Scientific Issues, Journal of Geophysical Research 107 (A12), ISSN 0148-0227, doi:10.1029/2002JA009430.

[32] A. Hedin, E. Fleming, A. Manson, F. Schmidlin, S. Avery, R. Clark, S. Franke, G. Fraser, T. Tsuda, F. Vial, R. Vincent, Empirical wind model for the upper, middle and lower atmosphere, Journal of Atmospheric and Terrestrial Physics 58 (13) (1996) 1421–1447, ISSN 00219169, doi:10.1016/0021-9169(95)00122-0.

[33] D. P. Drob, J. T. Emmert, G. Crowley, J. M. Picone, G. G. Shepherd, W. Skinner, P. Hays, R. J. Niciejewski, M. Larsen, C. Y. She, J. W. Meriwether, G. Hernandez, M. J. Jarvis, D. P. Sipler, C. A. Tepley, M. S. O'Brien, J. R. Bowman, Q. Wu, Y. Murayama, S. Kawamura, I. M. Reid, R. A. Vincent, An empirical model of the Earth's horizontal wind fields: HWM07, Journal of Geophysical Research: Space Physics 113 (12) (2008) 1–18, ISSN 21699402, doi:10.1029/2008JA013668.